J. Phys. France **49** (1988) 1017-1025 JUIN **1988,** PAGE 1017

Classification
Physics Abstracts
07.60F — 68.15 — 81.15L — 82.70G

Optical sol-gel coatings : ellipsometry of film formation

Alan J. Hurd and C. Jeffrey Brinker

Sandia National Laboratories, Albuquerque, NM 87185, U.S.A.

(*Reçu le 7 septembre 1987, révisé le 2 décembre 1987, accepté le 3 décembre 1987*)

Résumé. — On présente une méthode permettant de visualiser par ellipsométrie une région d'un film en train de sécher dans le procédé de dépôt par immersion ; cette méthode donne l'épaisseur du film et son indice de réfraction en fonction de la position. Les mesures préliminaires effectuées sur des sols alcooliques de TiO_2 et de SiO_2 indiquent que le film tend vers une fraction volumique d'environ 0,2 à l'état humide et suggèrent que le film résiste à une densification ultérieure pour des raisons cinétiques. Dans les films denses, le passage du front de séchage final produit un effondrement rapide du film sous l'effet des forces capillaires ; dans les films poreux formés de grands agrégats de SiO_2, l'affaiblissement final du film est plus lent parce que les forces capillaires sont plus faibles. Les profils d'épaisseur indiquent que l'amincissement du film résulte d'une combinaison de l'évaporation et de l'écoulement gravitationnel.

Abstract. — A method was developed to image an area of a drying, steady-state film during dip-coating using ellipsometry, thereby obtaining the film's thickness and refractive index as a function of position. Measurements on TiO_2 and SiO_2 alcohol-based sols indicate that the film approaches a volume fraction $\phi \sim 0.2$ in the wet state and suggests that the film resists densifying further for kinetic reasons. In dense films, as the final drying front passes, the film undergoes a rapid collapse owing to capillary forces ; porous films formed from relatively large SiO_2 aggregates appear to collapse more slowly in the final stage due to smaller capillary forces. The thickness profiles are consistent with thinning by a combination of evaporation and gravitational draining.

1. Sol-gel coatings.

Sol-gel coatings are applied to a wide variety of materials requiring high quality optical films [1, 2]. Since the coating can be formed simply by controlled dipping of the work followed by drying, difficult shapes and large sizes can be accommodated. By controlling the chemistry and the structure of the precursor sol, unusual materials can be applied and final film characteristics can be tailored to the requirements of a given application. A good example of the use of sol-gel dip coating is the application of interference coatings to large (1 m diameter) laser optics for which spin coating is not feasible and evaporative coatings are expensive. Another example of more industrial importance is the production of reflective window glass often seen in high-rise office buildings.

An important feature of sol-gel coatings is the ability to control the refractive index through variations of the sol ; this is particularly important when some interference condition is desired, e.g. multilayer dielectric coatings. Physical and chemical parameters can be used to vary the film. For example, by pre-aggregating the sol, a porous film with a low index results [3].

When a sol film dries, it passes through states of increasing solids concentration. In many cases the drying drives the film rapidly to gelation. In the precision dip-coating of photographic film, for example, a gelatin is used that quickly sets into a thick gel film. In the optical films studied here, the wet film dries quickly into a relatively thin layer and may pass through a transient gel-like state just before the final drying front passes [4]. By analogy to other colloidal systems, the film's viscosity and elastic modulus are expected to increase. This state determines many of the properties of the dry film ; in particular, the porosity is a function of the ability of the « gel » state to withstand collapse under the

capillary forces of the drying front. A major goal of this study is to understand the nature of this fleeting gel-like state and how the microstructure of the final film evolves from it.

A second interesting goal is the measurement of film drainage thickness in the presence of vigorous evaporation. The great importance of dip coating in many aspects of manufacturing has spawned an extensive literature on the theory [5-7] and measurement [8, 9] of gravitational draining of plates and wires. The drainage problem arises in such disparate fields as volumetric measurement and nuclear reactor safety (where the cooling of reactor walls depends on a draining film). It appears that no one has yet addressed the case of draining with evaporation theoretically, although it is clearly an important dip-coating situation.

Since the instantaneous volume fraction is a key parameter in the film properties, a natural quantity to measure is the refractive index, which can be related to the volume fraction through a number of optical models. Although ellipsometry is well suited for thin, locally homogeneous layers of unknown index and thickness, the common methods of using a small localized beam to probe the sample are inadequate due to fluctuations in the film from dust and convection. For this reason, a specialized ellipsometer was developed to probe many points and many combinations of index and thickness at once.

The purpose of this paper is mainly to describe the apparatus. Data on optical films are given although their analysis is not exhaustive.

2. The film.

Good quality films were made with the film-drawing apparatus shown in figure 1. In this apparatus, a long narrow substrate (1 cm × 10 cm) cut from a silicon wafer was slowly drawn out of a sol reservoir by the smooth hydraulic action of draining a large cylinder through a controlled orifice. A float on the draining liquid's surface pulled the substrate *via* a pulley system. The speed V of withdrawal could be varied from 0 to 0.3 cm s^{-1}.

With volatile solvents, a steady-state film profile was rapidly achieved for which the velocity of the drying front matched the withdrawal velocity ; this state lasted long enough (1 min) to make measurements. The substrate was enclosed to reduce convection and to maintain a well defined level of solvent saturation above the sol reservoir.

The chemical flexibility of the sol-gel coating process allows for a wide variety of materials to be deposited. In these studies, we have used titanate and silica sols, which are both widely employed in optical applications.

Titania sols (4.9 % equivalent wt. TiO_2) were prepared by partially hydrolyzing titanium ethoxide,

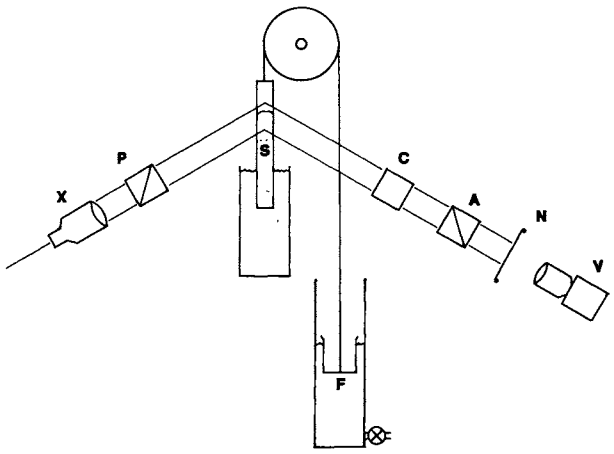

Fig. 1. — Sol-gel film-drawing apparatus and ellipsometer. The reflective silicon substrate S is slowly pulled from a reservoir containing a dilute sol using a hydraulic movement created by a floating cup F on a reservoir draining through a controlled orifice. The ellipsometer consists of a beam expander X, a polarizer P, a $\lambda/4$ compensator C, an analysing polarizer A, a diffusing screen S and a video camera V. The polarizers are motorized.

$Ti(OC_2H_5)_4$, in an acidic (HCl) solution of ethanol using a molar ratio of $H_2O/Ti = 1$. The partially hydrolyzed species condensed to form titanate oligomers composed of Ti-O-Ti bonds. Small-angle X-ray scattering measurements indicated that the titanate oligomers were ~ 10 Å in diameter.

It is not certain how to model the refractive index of these oligomers in solution. We have used effective medium theories (discussed below), with the assumption that the titanate particles have a refractive index of 2.2. This assumption remains an important source of uncertainty in the determination of solids volume fraction in the drying films.

During film formation, continued hydrolysis occurs on contact with atmospheric moisture leading to additional condensation. The as-deposited titanate films had a refractive index around 1.7 (corresponding to a volume fraction of the proposed oligomers of 66 % and 34 % porosity), which increased to 2.2 after heating for 5 min at 450 °C. The film thickness decreased by 30 % to 40 % during heating, corroborating the porosity value and lending support to the assumed index of the oligomers.

The silica sols were comprised of colloidal suspensions of 150-200 Å diameter silica spheres made by a variation of the Stöber process utilizing 2.5 moles H_2O/mole Si. Films drawn from stable, monodisperse suspensions of 3 % (wt) silica at pH 10 had a refractive index of about $n = 1.25$ before baking. Low index films, $n = 1.16$, were deposited from pre-aggregated silica sols obtained by reducing the pH to 7 using HCl ; the low index reflects the ramified nature of the individual aggregates prior to deposition.

3. The ellipsometer.

A beam of light reflecting from a surface suffers different amplitude and phase shifts in its « s » (polarization parallel to surface) and « p » (polarization perpendicular to surface) waves. In ellipsometry [10], these amplitude and phase shifts are measured then interpreted by an appropriate model. A typical ellipsometer consists of a laser, a polarizer to prepare a known polarization, the reflecting sample, a $\lambda/4$ compensator plate that resolves the s and p waves, and an analysing polarizer. The analyser and polarizer are adjusted until the reflected beam is extinguished.

The angle of the polarizer determines the relative amplitudes of the incident s and p waves ; its angle at extinction compensates for the difference in s and p reflection amplitudes. With the compensator's fast axis at 45° to the plane of incidence, the analysing polarizer, when tuned to extinction, measures the angle at which the reflected light must pass through the $\lambda/4$ plate to compensate for the phase shift difference suffered by the s and p waves. With the two polarizer angles measured at extinction, it is possible to calculate both the index n and thickness h of a film covering a substrate with a known index. Since each polarizer has two equivalent positions, there are four possible extinction conditions, or four « zones ».

In the case of the silicon wafers used here, the substrate index is complex. Periodically, two-zone measurements were made on uncoated substrates to check the real and imaginary index values, which were found to be $\mathrm{Re}(n) = 3.856$ and $\kappa = \mathrm{Im}(n)/\mathrm{Re}(n) = 0.052$, and to monitor the precision of the apparatus. Although these values are within the range of accepted values for clean silicon, the silicon surface inevitably has an oxide layer that endows the substrate with the wetting properties of silica appropriate for many optical applications.

In these experiments the angle of incidence was fixed at 67.5° and the wavelength was 6 328 Å.

The usual methods of narrow-beam ellipsometry were found to be unsatisfactory in our initial attempts to study films because of fluctuations in thickness. Furthermore, it was desirable to obtain data from many points on the film at once rather than one point per dip coating. Hence, the laser was expanded and collimated to illuminate approximately 1 cm^2 of the film (an area limited mainly by the apertures of the polarizing optics). In a sense, each ray in the expanded beam defined its own ellipsometer, probing the film point-by-point (diffraction notwithstanding) and forming a « phase » image of the film.

The fluctuations appeared to be mainly the result of residual atmospheric convection near the sample in spite of our attempts to isolate the sample in a chamber. (Occasionally dust on the substrate was also a problem.) The drying front would recede and advance randomly by $\pm 100\ \mu$ from its average position in the laser beam on time scales of 5-10 s. Since the wedge angle of the drying film was 10^{-3} radians, these fluctuations corresponded to thickness variations of ± 100 Å at a given spot on the film (in the lab frame of reference) and were enough to destroy the interference conditions for extinction. It was too difficult to find the polarizer angles for an extinction in the short time that the film was steady.

With the expanded beam, however, clear images were seen of the drying film. These images, seen in figure 2, consisted of nonlocalized fringes, like shadows, whose sharpness was degraded by diffraction to a greater degree the further out the image was projected from the sample. By intercepting the image with a diffuse screen as close to the substrate as possible, however, good spatial resolution (~ 50 μm) was possible. Although better resolution could be attained by using focusing lenses [11, 12], the gains would require introducing a spread in incident angle and an attendant uncertainty in the measured index [12] as well as additional optical elements to complicate our analysis.

For arbitrary polarizer settings, the corresponding thickness and index required for a null would be present somewhere in the image only by chance. The problem was to find polarizer settings that gave extinctions somewhere on the continuously varying film. Obviously it is difficult, if not impossible, to explore all polarizer-analyser settings (corresponding to index-thickness combinations) on such short-lived films but strategies could be devised to look for nulls in certain ranges of thickness.

The idea is best illustrated by figure 3, showing the locus of extinctions in the $\Delta - \Psi$ plane, where Δ and Ψ are the classical ellipsometric angles and are related in simple ways to the angles of the analyser A_p and polarizer P_p [13]. (When the analyser and polarizer angles are between 0° and 90° from the plane of incidence, $\Delta = -90° - 2A_p$ (mod 360°) and $\Psi = P_p$.) A roughly elliptical figure in the $\Delta - \Psi$ plane defines those polarizer settings at which an extinction is expected for a given film index n_1. As the film thickness increases, the null points progress counterclockwise around the ellipse, starting with the leftmost point A at zero thickness. After a certain thickness is exceeded, the optical conditions repeat ; therefore it is impossible to distinguish between thicknesses differing by integer multiples of this optical phase thickness (one-half the wavelength inside the medium, approximately 2 500 Å) without additional information as to the order of the extinction. For another index of refraction n_2, the ellipse is distinct except at point A where all ellipses meet.

Now, a drying sol-gel film consists of continuously varying thicknesses and indexes falling somewhere

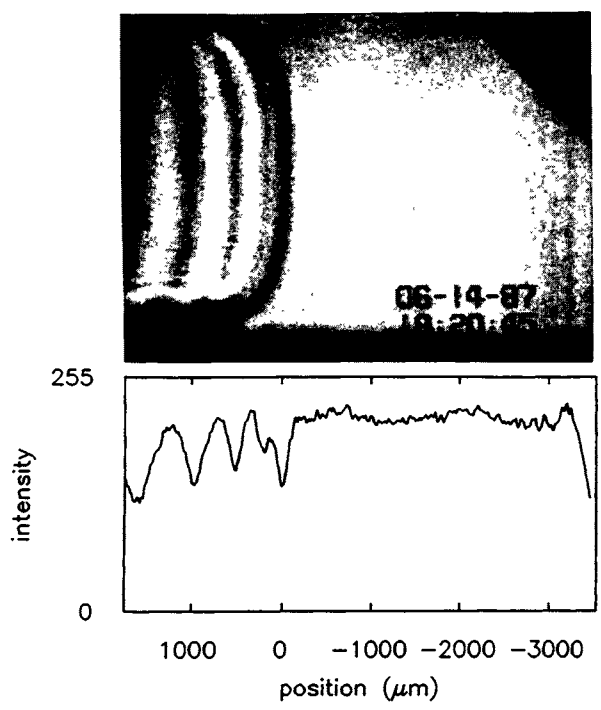

a)

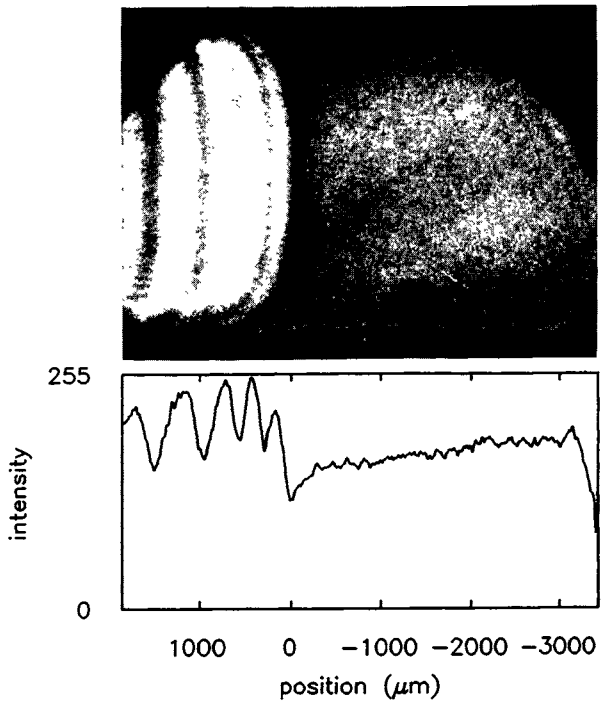

c)

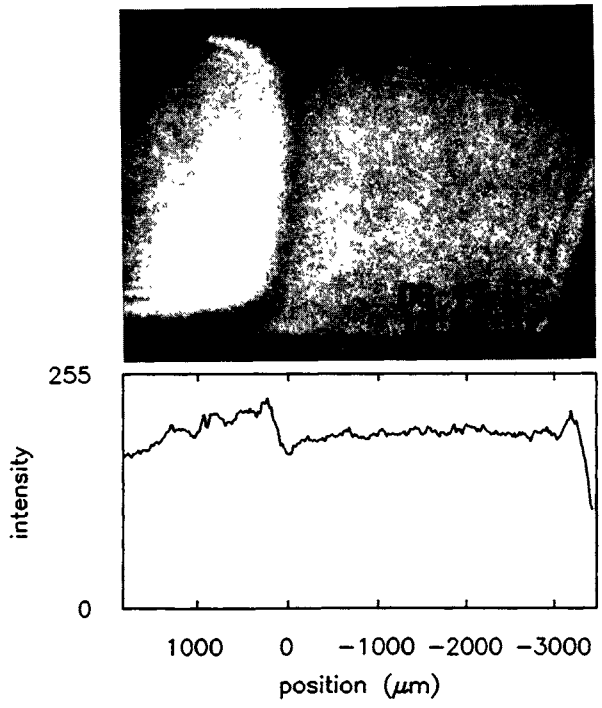

b)

Fig. 2. — Ellipsometric images of drying films with different analyser positions. The frames were recorded at the positions A, B and C in figure 3. a) At A, the fringes correspond to optical thickness fringes of integer multiples of $\lambda/2$; b) at B, no extinctions are possible and none are seen ; c) at C, the first fringe is passing through a minimum (something that can be determined only by comparison of adjacent video frames) allowing the calculation of the index and thickness along that contour.

between the ellipses for n_1 and n_2, say, and it is impossible to know beforehand where to look in the $\Delta - \Psi$ plane for an extinction. By continuously rotating one or both polarizers, however, a path can be described in the plane that guarantees passage through a null condition. One such path is ABCD shown in figure 3 for which the analyser is held constant while the polarizer is changed continuously with a motor. In the ellipsometric image, this change is manifested as a variation in darkness of the fringes running through the film, shown in figure 2. When the extinction condition for a given thickness is met, the intensity passes through a minimum for one or more fringes. Knowing the polarizers' positions for

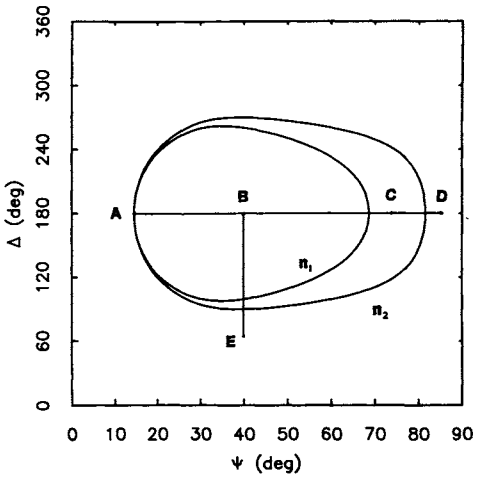

Fig. 3. — Locus of extinctions as function of ellipsometric angles Δ and Ψ (related to polarizer angles) for indexes n_1 and n_2 (solid curves, with $n_1 < n_2$) and spatially varying film index (dashed curve). Motorized polarizers allow searching along paths that guarantee crossing an extinction in the film.

this condition, along with the order of the fringe, allows the calculation of both the index and the thickness unambiguously.

In practice it is not easy to identify the points of minimum intensity. Image processing was used on video recordings of the ellipsometric image to accomplish this. The intensity profile normal to the fringes was calculated by averaging up to 10 pixels (~ 70 μm) on either side of a line perpendicular to the fringes. Thus the resolution perpendicular to the dipping direction was coarse (> 150 μm) but fairly high (~ 50 μm) along the dipping direction. This averaging procedure provided a smooth representation of the fringe profile. Each profile was normalized by the average image intensity in order to remove gain changes introduced automatically by the video camera electronics when the overall intensity changed. By monitoring the depth of the fringes as a function of time, the intensity minimum could be identified and correlated with the polarizer setting to within 1°. Using a one-layer optical model [10], the thickness and index uncertainties were typically 1 %. The fringe position along the substrate was referred to an intensity peak or valley near the drying front tip rather than to the absolute pixel coordinates in the video image because the film's position would often fluctuate while its profile would remain constant.

Different paths in the $\Delta - \Psi$ plane provided information at different thicknesses in the film. Hence, the path BD in figure 3 gave fringes at thicknesses of approximately 1 200 Å, 3 600 Å, 6 000 Å, ... whereas the path BE gave fringes at approximately 600 Å, 3 000 Å, 5 400 Å, ...

Only at places on the film corresponding to one set of thicknesses at a time can null ellipsometry provide the refractive index. In principle, the intensity can be used to evaluate the index and thickness without finding a null condition [10, 12] ; but the necessary measurements require absolute intensity calibration which was not possible with the automatic gain circuitry in our video camera. This remains a promising avenue of improvement.

4. Results.

Knowing the index of refraction for the constituents of the film, various optical models can be used to calculate the volume fraction of solids [14]. A well known theory is the effective medium model by Maxwell Garnett, which assumes that there are identifiable particles of one material inside a matrix of another and takes their (optical) interactions into account by a mean-field procedure. Another model at the same order of approximation is the Bruggeman theory, developed to describe two-component mixtures rather than a particulate medium. Presumably, the Maxwell Garnett theory is more appropriate for the silica colloidal sols whereas the Bruggeman theory is better for the titania polymeric sols. In practice, however, both theories gave the same answers to within experimental error for the data at hand. A third possibility, the Lorentz-Lorentz relation, also agrees well with these approximations. For our purposes, only the Maxwell Garnett predictions are discussed. The particle volume fraction is given in this theory by

$$\phi = \left(\frac{n_a^2 + 2 n_b^2}{n^2 + 2 n_b^2} \right) \left(\frac{n^2 - n_b^2}{n_a^2 - n_b^2} \right), \qquad (1)$$

where n_a and n_b are the indexes of the particles and solvent, respectively, and n is the measured index of the film.

Figure 4 shows the TiO_2 film's index as a function of thickness, and figure 5 is the thickness as a function of position on the film using a path of the type ABCD and a withdrawal speed of $V = 0.096$ cm/s. From equation (1), the volume fraction of titania could be calculated assuming a completely wet film. ϕ is plotted in figure 6 using an index of 2.2 for the titania sol particles and 1.35 for the solvent index.

Shown in figures 4-6 are solid curves corresponding to constant removal of solvent by evaporation and, in figure 5, a dashed curve for a case of interrupted gravitational draining (discussed below). The thickness profile is curved in a way that implies a combination of evaporation and gravitational draining.

Note that there is an offset of 63.8 μm implied by the x-intercept of the solid line : the position along the film was measured against an arbitrary optical

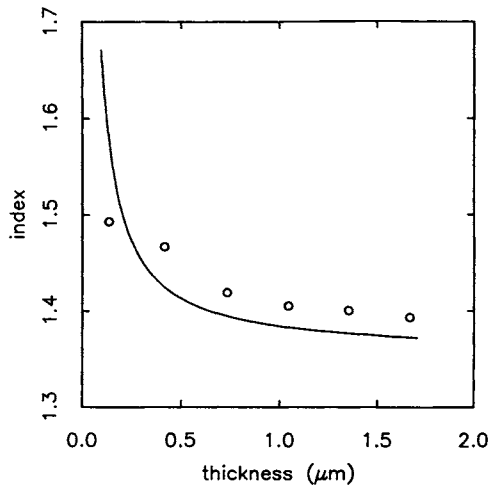

Fig. 4. — Index-thickness curve of drying titanate film. The solid line represents the index expected for constant evaporation and no gravitational draining.

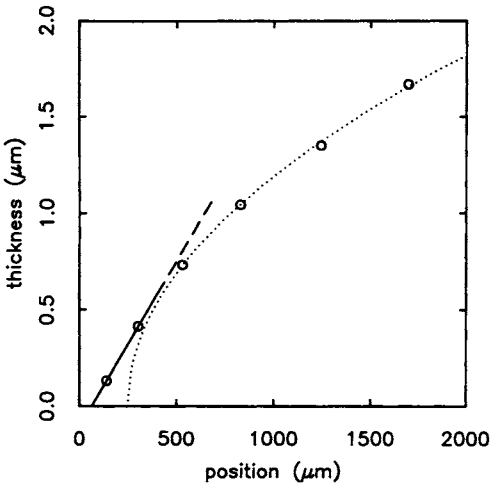

Fig. 5. — Thickness profile of drying titanate film. The displacement along the film was measured from a fiducial point near the drying front. The solid line represents a constant evaporation profile with no gravitational draining or other effects. The dotted line is the profile for gravitational draining but no evaporation.

feature (intensity minimum or peak) associated, but not necessarily coincident, with the leading edge of the wet film. This choice of origin was arbitrary but it is clear from figure 5 that the edge of the bulky wet film can be identified to within 10 μm by extrapolation. On the other side of the edge, the « dry » film may still be somewhat wet in many cases, particularly the pre-aggregated SiO_2 sols ; but judging from the images it appeared that beyond the extrapolated edge or drying front the solvent was largely gone. If the substrate was suddenly stopped the wet film would recede from view and the intensity of the image of the coated substrate would not change with time.

The most notable feature of the index data, figure 4, is that close to the drying front (within 150 μm) the index does not exceed 1.5, implying a maximum volume fraction of $\phi = 0.20$ as shown in figure 6. A similar maximum wet volume fraction

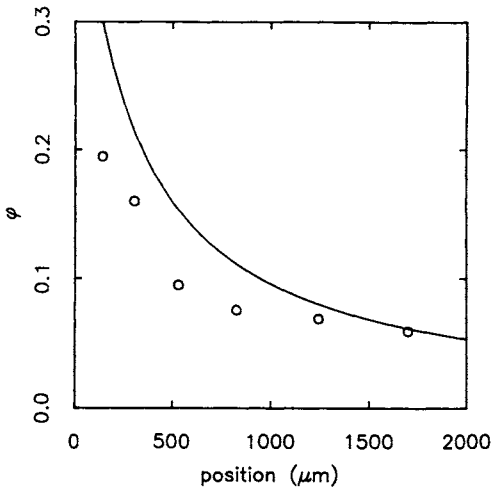

Fig. 6. — Profile of volume fraction of solids of drying titanate film from equation (1). Note that the volume fraction lags behind the expectation for constant evaporation and no draining (solid line).

was seen in the SiO_2 monodisperse and pre-aggregated sols. With the exception of the pre-aggregated SiO_2 sol, the films transformed rapidly in the final 150 μm to become dry, compact films with solid volume fractions around 60 %. The pre-aggregated SiO_2 sol exhibited a very slow final drying as seen optically by a bright « plume » at the tip in figure 7.

5. Time scales.

First, it is helpful to establish that the films are most likely uniform in their thickness direction. One might worry, for example, that the evaporation might lead to a concentrated layer near the liquid-air surface that would invalidate the ellipsometry model, among other things.

In fact, the time necessary for the largest particles to diffuse across the layer is small, as can be seen by the following estimates. When the film is dilute enough that the viscosity η can be taken as that of the solvent, the self-diffusion constants $D = kT/(6\pi\eta a)$ of the TiO_2 species ($a < 20$ Å), the SiO_2 spheres ($a = 200$ Å) and the SiO_2 aggregates ($a = 2\,000$ Å) are 10^{-6}, 10^{-7} and 10^{-8} cm^2/s, respectively. For a film thickness of about 1 μm, the times for diffusing across the film are 2, 20 and 200 ms, respectively, and for a withdrawal speed of

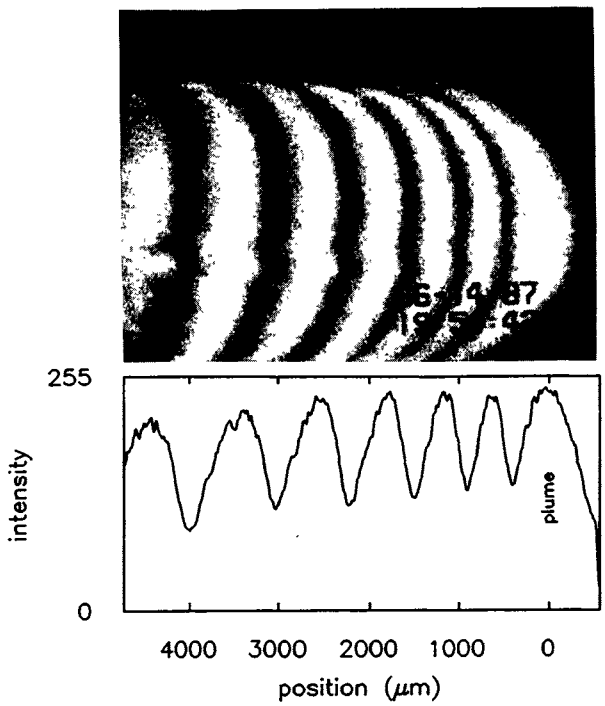

Fig. 7. — Tip of drying film of pre-aggregated silica colloid. Note the extensive « plume » where the film is slowly thinning down by evaporation and collapse under surface tension.

0.1 cm/s, the distance along the substrate over which the relaxation takes place is at most 100 μm, which is comparable to the current resolution. Thus, if an inhomogeneity developed, we would not have the resolution to be affected by it. For more concentrated parts of the film, the mutual diffusion must be used [15] but up to the volume fractions of 30 % these estimates vary by about a factor of two. We conclude, therefore, that concentration gradients in the thickness direction are not important for most of the film. Regions of $\phi > 0.3$ were narrower than our resolution. In any case, the one-layer model we have adopted for interpreting the ellipsometric angles assumes homogeneity, and therefore returns an index averaged over the thickness.

The continual loss of solvent in the drying film implies a contraction of the interparticle separations. If this convective transport is large compared to diffusional transport, then concentration fluctuations will have no time to relax by diffusion and the system might end up in a glassy metastable arrangement. On the other hand, if diffusion is given time to act at all stages of drying, the structure would be dictated by diffusion-limited or reaction-limited processes.

In actuality, under the assumption of constant evaporation, the transport by evaporative contraction is very slow compared to Brownian motion, at least until the viscosity begins to diverge significantly. It is easy to see that the average particle separation varies as the cube root of the inverse thickness, $\langle r \rangle$ = (number density)$^{-1/3}$ = (film area)$^{1/3}$ $h^{1/3}$. Assuming a constant thinning by evaporation from some initial thickness h_i such that $h = h_i - bt$, a typical contraction of $\langle r \rangle$ by evaporation is given by $\Delta r = (\Delta \langle r \rangle^3)^{1/3} \sim t^{1/3}$, which is a smaller power than $\Delta r \sim t^{1/2}$ for diffusion. The linear profile assumed here for h is incorrect (Fig. 5) but good enough in the thick parts of the film to compare time scales.

6. Profile.

Three major factors control the film thickness profile : hydrodynamic flow owing to gravitational draining, solvent evaporation, and the viscoelastic properties of the entrained fluid, including the effects of the sol on the solvent. It is possible that surface-tension forces influence the amount of sol initially entrained near the bottom meniscus [5] and that osmotic and electric double-layer forces influence the profile in its late stages ; but these effects should be less important than the first three.

In the absence of evaporation, a steady-state fluid film on a plate drawn continuously from a bath would have a constant thickness given by [6]

$$h_0 = (\eta V/\rho g)^{1/2} \approx 10\ \mu\text{m}\ , \qquad (2)$$

where η is the viscosity (0.01 poise), V is the withdrawal speed (0.1 cm/s), ρ is the density (1 gm/cc) and g is the acceleration due to gravity (980 cm/s^2). If the film were suddenly stopped, the profile below the uncoated area would be [7]

$$h(x, t) = h_0 (x/Vt)^{1/2}\ , \qquad (3)$$

where x is the distance from the tip. The case of draining with evaporation has apparently not been solved.

It is interesting to compare equation (3) with the data to test the assumption that the profile develops quickly according to (3) then ablates uniformly by evaporation until a steady-state is achieved. (This is crude reasoning since the governing equations don't admit a steady-state solution of the form (3).) The dotted line in figure 5, following equation (3), and the solid curve, describing purely evaporative thinning, show that the truth lies in between : the film profile is a combination of gravitational draining and evaporation.

While the gravity-induced flow affects the amount of solids entrained at the withdrawal point and therefore the dry-film thickness, it does not directly change ϕ or the index n : the evaporation process is the mechanism that drives the film to more and more concentrated conditions. As the film dries and the viscosity and elastic modulus become important, then the gravitational flow conditions may change enough to affect the thickness profile but still should

not change the wet-film index. For this reason the evaporation model, assuming constant removal of solvent, describes the index profile fairly well as long as the solids content is low enough that the evaporation rate is that of the solvent. Near the drying front, the increasing viscosity and elasticity might slow down the thinning rate, allowing an open structure to freeze in.

7. Evaporation.

The evaporation rate may not be constant everywhere on the film. Locally, the evaporation rate would be expected to decrease in the more concentrated areas of the film because the solute particles constitute barriers to the solvent for diffusing to the surface in order to evaporate. Also, if dry sol particles occupy part of the surface, then the area available for evaporation decreases. This decreasing evaporation trend is followed in reference [16] from 25-50 % volume fraction of latex particles in water with a laminar gas flow over the film, much like the case of continuous withdrawal. Between 50 % and a closest packing of 74 %, the evaporation rate is constant but not too different from that of the solvent (perhaps a factor of 2 slower), and below 25 % the evaporation rate is close to that of the solvent. Therefore, in our films we expect little variation for most of the wetted area since the volume fraction in most measured locations is small.

In all the runs of the titania sol and the unaggregated silica sol, the final volume fraction observed was only $\phi = 0.2 \pm 0.1$ for our measurements closest to the drying front [17]. (At present the closest we can observe to the drying front is about 50 μm although improvements in the apparatus to eliminate diffraction should decrease this limitation significantly.) Furthermore, the change in ϕ appeared to be decreasing near the tip. Apparently the densification of the wet film is mechanically « forbidden » to increase much further, probably due to the divergence of the viscosity. In gelling systems, it is well known that the viscosity diverges with a power law in the reaction time [18, 19] and hence with the free volume fraction occupied by the sol ; even in nongelling, stable colloids an infinite cluster appears in sheared suspensions at $\phi \sim 0.20$, analogous to percolation, that leads to plug flow [20]. These considerations suggest that the nature of the final wet state is like a gel in structure and elastic properties, having extensive connectivity. Furthermore, the gel *time*, describing the time required to reach the viscosity singularity [19], is inversely proportional to a power of the concentration for some types of kinetic gelation [21]. Thus, in the proposed concentration-induced gelation of a drying film, the evaporation leads inevitably to a sol that very quickly « gels » in the sense that the viscosity diverges dramatically ; whether the final state has time for diffusional relaxation remains to be seen.

Since it is apparent that very rapid changes occur in the final drying, this gel-like state is not necessarily long-lived. In the monodisperse sols, it lived no longer than 2 ms before drying completely. If all the solvent in the gel-like state, $\phi \approx 0.2$, were to be replaced by vacuum, the index would of course *decrease* from around 1.5 to 1.3 if there were no further collapse of the film. Instead the index increased from 1.5 to 1.7 ; clearly there must be a substantial collapse as the drying front passes, probably owing to the existence of large capillary forces in the porous film as small-diameter menisci retreat.

The unaggregated silica system exhibited behaviour similar to the titania sol. It is difficult to detect changes in the refractive index in the silica sols because the index of silica is not very different from that of the solvent (1.48 vs. 1.35). In any case, the silica sol densified up to $\phi \approx 0.2$ while still wet then rapidly dried to a dense film with $\phi \approx 0.6$.

The pre-aggregated silica sol exhibited somewhat different drying characteristics near the tip. There was evidence of an extensive, long-lived, wetted state as illustrated by a bright « plume » in figure 7. This plume represented a thin but slowly changing plateau in the thickness profile. Because the pores in the film were large, the capillary forces generated by the menisci of the retreating solvent were small. It may also be that the large relatively thickness of these porous films impeded the evaporation of solvent more than in the other sols. (Typically, the pre-aggregated sols yielded films of thickness 2 100 Å compared to 800 Å for the unaggregated sol.) Apparently the aggregates in the film were fairly stiff because they did not collapse completely into a close-packed film upon final drying. Far from the tip, where the film was thick, the profile was similar to those of the other sols.

The scattering from the plume area appeared to be relatively large during the course of the experiments. We note that experiments on the drying of particle compacts have uncovered complex, diffuse boundaries of the type that might lead to such scattering [22]. Elsewhere in the image, the samples did not appear to scatter light strongly enough to influence the ellipsometric measurements since crisp images of the film were always seen.

8. Conclusions.

We have demonstrated an imaging ellipsometer that allows simultaneous measurements of the index and thickness profiles of a drying film. For continuously withdrawn sol-gel coatings, the index appears to increase by solvent evaporation to a value corresponding to a volume fraction of approximately 0.20, at which point the film may be in a gel-like

state of high viscosity and elasticity. When the final drying front passes, the film collapses by surface tension into a dry film that generally has a higher final index than the wet film, although the final index is lower for the porous films formed by aggregated silica particles.

Future experiments will probe the film closer to the drying front. Of particular interest is the index and thickness of the pre-aggregated films in the fluffy plume region. Experiments are planned to map the fluid velocity profile using optical labeling techniques for a direct measure of the viscosity and to establish the existence or absence of plug flow.

Acknowledgments.

It is a pleasure to thank Herb Tardy and Tom Christensen of Sandia Labs for expert advice on ellipsometry, particularly for helpful analysis programs. Enormous credit is owed to Scott Reed and Carol Ashley, for the film-drawing apparatus and materials, and to Dave Evans for image processing software, all Sandians. Special thanks to Dick Eley of Glidden for helpful discussions. This work was performed at Sandia National Laboratories under the Department of Energy contract No. DE-AC-04-76DP00789.

References

[1] SCHRÖDER, H., in *Physics of Thin Films : Advances in Research and Development*, Eds. G. Haas and R. E. Thun **5** (1969) 87.

[2] DISLICH, H., *J. Non-Cryst. Solids* **73** (1985) 599.

[3] BRINKER, C. J., KEEFER, K. D., SCHAEFER, D. W., ASSINK, R. A., KAY, B. D. and ASHLEY, C. S., *J. Non-Cryst. Solids* **63** (1984) 45.

[4] BRINKER, C. J., HURD, A. J. and WARD, K. J., in *Proceedings of the 3rd International Conference on Ultrastructure Processing of Ceramics, Glasses and Composites*, Eds. J. D. Mackenzie and D. R. Ulrich (Wiley-Interscience, New York) 1988.

[5] LANDAU, L. and LEVICH, B., *Acta Physicochim. URSS* **17** (1942) 42 ;
DERYAGIN, B. M. and LEVI, S. M., *Film Coating Theory* (Focal Press, New York) 1964.

[6] TUCK, E. O., *Phys. Fluids* **26** (1983) 2352.

[7] JEFFREYS, H., *Proc. Cambridge Phil. Soc.* **26** (1930) 204.

[8] LANG, K. C. and TALLMADGE, J. A., *Ind. Eng. Chem. Fundam.* **10** (1971) 648.

[9] SCHLESINGER, M., DE KEE, D. and GODO, M. N., *Rev. Sci. Instrum.* **57** (1986) 2535.

[10] AZZAM, R. M. A. and BASHARA, N. M., in *Ellipsometry and Polarized Light* (North-Holland, Amsterdam) 1977, chapter 4.

[11] KODAMA, T., *Denki Kagaku* **42** (1974) 344.

[12] ERMAN, M. and THEETEN, J. B., *J. Appl. Phys.* **60** (1986) 859.

[13] For our polarizer-sample-compensator-analyser arrangement, the intensity extinctions occur when

$$r_p/r_s = \tan \Psi \, e^{i\Delta} = \\ = - \tan P_p \frac{\tan C + \rho_c \tan (A_p - C)}{1 - \rho_c \tan C \tan (A_p - C)},$$

where r_p and r_s are the reflection coefficients for p and s polarizations, ρ_c characterizes the compensator, and C is the angle of the compensator's fast axis. For a $\lambda/4$ plate at 45°, $\rho_c = e^{-i\pi/2}$, $C = \pi/4$, and

$$\tan \Psi \, e^{i\Delta} = \tan P_p \, e^{i(\pm 2\pi + \pi - 2A_p)},$$

or $\Psi = P_p$ and $\Delta = -90° - 2A_p$ (mod 360°) as stated in the text.

[14] BOHREN, C. F. and HUFFMAN, D. R., in *Absorption and Scattering of Light by Small Particles* (Wiley-Interscience, New York) 1983, chapter 8.

[15] BEENAKKER, C. W. J. and MAZUR, P., *Phys. Lett.* **91A** (1982) 290 ;
PUSEY, P. N. and VAN MEGEN, W., *J. Phys. France* **44** (1983)

[16] POEHLEIN, G. W., VANDERHOFF, J. W. and WITMEYER, R. J., *Polym. Prepr., Am. Chem. Soc., Div. Polym. Chem.* **16** (1975) 268.

[17] This conclusion is somewhat sensitive to the optical properties assumed for the sol, in particular the index of refraction of the oligomers or spheres in suspension. In the titanate films, the largest limiting volume fraction consistent with any reasonable assumptions is 0.4 ; here we adopt the model most consistent with our data as outlined in section 2.

[18] ZALLEN, R., in *The Physics of Amorphous Solids* (Wiley-Interscience, New York) 1983, ch. 4.

[19] GAUTHIER-MANUEL, B., GUYON, E., ROUX, S., GITS, S. and LEFAUCHEUX, F., *J. Phys. France* **48** (1987) 869 ;
SAKKA, S. and KAMIYA, K., *J. Non-Cryst. Solids* **48** (1982) 31.

[20] DE GENNES, P. G., *J. Phys. France* **40** (1979) 783.

[21] HENDRIKS, E. M., ERNST, M. H. and ZIFF, R. M., *J. Stat. Phys.* **31** (1983) 519. Although the gel time depends critically on the interactions between colloidal species, the Smoluchowski coagulation equation suggests that the gel time varies inversely with initial concentration for certain kernels, all other things being equal. This point does not appear to have been verified or widely studied experimentally. (But see Sakka and Kamiya (1982), Ref. [17].)

[22] SHAW, T. M., in *Better Ceramics Through Chemistry II*, Eds. C. J. Brinker, D. E. Clark and D. R. Ulrich (Materials Research Society, Pittsburgh) 1986, p. 215.